Neural Networks 66 (2015) 79–90

Contents lists available at ScienceDirect

Neural Networks

journal homepage: www.elsevier.com/locate/neunet

A digital implementation of neuron–astrocyte interaction for neuromorphic applications

Soheila Nazari [a], Karim Faez [a], Mahmood Amiri [b,*], Ehsan Karami [c]

[a] Department of Electrical Engineering, Amirkabir University of Technology, Tehran, Iran

[b] Medical Biology Research Center, Kermanshah University of Medical Sciences, Kermanshah, Iran

[c] Department of Electronic, Razi University, Kermanshah, Iran

ARTICLE INFO

Article history:
Received 12 September 2014
Received in revised form 8 January 2015
Accepted 25 January 2015
Available online 2 February 2015

Keywords:
Neuron–astrocyte interactions
FPGA
Neuromorphic
Linear approximation

ABSTRACT

Recent neurophysiologic findings have shown that astrocytes play important roles in information processing and modulation of neuronal activity. Motivated by these findings, in the present research, a digital neuromorphic circuit to study neuron–astrocyte interaction is proposed. In this digital circuit, the firing dynamics of the neuron is described by Izhikevich model and the calcium dynamics of a single astrocyte is explained by a functional model introduced by Postnov and colleagues. For digital implementation of the neuron–astrocyte signaling, Single Constant Multiply (SCM) technique and several linear approximations are used for efficient low-cost hardware implementation on digital platforms. Using the proposed neuron–astrocyte circuit and based on the results of MATLAB simulations, hardware synthesis and FPGA implementation, it is demonstrated that the proposed digital astrocyte is able to change the firing patterns of the neuron through bidirectional communication. Utilizing the proposed digital circuit, it will be illustrated that information processing in synaptic clefts is strongly regulated by astrocyte. Moreover, our results suggest that the digital circuit of neuron–astrocyte crosstalk produces diverse neural responses and therefore enhances the information processing capabilities of the neuromorphic circuits. This is suitable for applications in reconfigurable neuromorphic devices which implement biologically brain circuits.

1. Introduction

Astrocytes, the predominant type of glial cell in the central nervous system (CNS), have long been believed to provide only structural and metabolic supports (Koizumi, 2010). However, recent researches have demonstrated that astrocytes intervene actively in information processing and control of synaptic transmission (Kuga, Sasaki, Takahara, Matsuki, & Ikegaya, 2011; Papa, De Luca, Petta, Alberghina, & Cirillo, 2014). Bidirectional communications between astrocytes and neuronal cells are necessary for the normal functioning of the nervous system during signal processing (Dallérac, Chever, & Rouach, 2013). Although astrocytes cannot generate action potentials, they respond to neuronal activities with an elevation of their intracellular calcium levels. In this way, astrocytes can respond to neurotransmitters with calcium elevations that lead to the *release* of gliotransmitters including glutamate or ATP and generate feedback signals to neurons in order to modulate synaptic transmission between nearby neurons, neuronal excitability and to an extent also plasticity (Linne & Jalonen, 2014; Reato, Cammarota, Parra, & Carmignoto, 2012; Sasaki, Kuga, Namiki, Matsuki, & Ikegaya, 2011). In this way, the astrocyte "listens and responds" to the synapse and regulates normal operation of synapses via astrocytic mechanisms (Fellin, 2009; López-Hidalgo & Schummers, 2014). In recent studies, several analog and digital brain-inspired electronic systems have been recently proposed as dedicated solutions for fast simulations of spiking neural networks (Joshi, Parker, & Hsu, 2009; Pfeil et al., 2013). While the interest in understanding the biological operations and computational modeling of neuron–astrocyte signaling is continuously increasing, the neuromorphic neuron–astrocyte cross-talk circuit is less studied (Amiri, Bahrami, & Janahmadi, 2012a, 2012b; Amiri, Hosseinmardi, Bahrami, & Janahmadi, 2013a; Nazari et al., 2014). An increasing interest in neuron–astrocyte signaling has paralleled our development of neuromorphic circuits incorporating astrocytes (Joshi, Parker, & Tseng, 2011). Therefore, it is essential to develop digital and analog circuits which consider neuron–astrocyte signaling.

Although, the focus of this paper is to propose a digital neuron–astrocyte circuit to verify that the circuit can produce similar

* Correspondence to: Parastar Ave., Kermanshah University of Medical Sciences, Kermanshah, Iran.
E-mail address: ma.amiri@ece.ut.ac.ir (M. Amiri).

http://dx.doi.org/10.1016/j.neunet.2015.01.005
0893-6080/

responses as the biophysical model does, we present a first step in an ongoing effort to integrate the functional contribution of astrocytes in neuromorphic engineering which can be used as a platform for developing and emulating simple brain like computing system (Ambroise, Levi, Joucla, Yvert, & Saïghi, 2013; Cassidy, Georgiou, & Andreou, 2013). This also supports to understand how the astrocytes shape the neural information processing from hardware point of view. Therefore, in the present research, we have implemented a functional approach to develop a digital neuromorphic circuit and to explore the feasibility of using field-programmable gate arrays (FPGA) for implementing bidirectional communication neuron–astrocyte. Neuromorphic VLSI is an important tool for investigating and implementing neural algorithms. Recent studies in computational intelligence have shown a strong tendency towards a better understanding of biological systems and the details of neuronal signal processing. Such research is motivated by the desire to form a more comprehensive understanding of information processing in biological networks and to investigate how this understanding could be used to improve traditional information processing techniques (Misra & Saha, 2010). When we implement biological networks on hardware, we can take full advantage of their inherent parallelism and run orders of magnitude faster than software simulations, becoming thus, adequate for real-time applications. Since VLSI implementation cannot be reconfigured easily (Indiveri & Horiuchi, 2011; Wijekoon & Dudek, 2012), here we chose FPGAs for hardware implementation. FPGAs are devices that permit the implementation of digital systems, providing an array of logic components that can be configured in a desired way (Sepulveda, Muñoz, Espinoza, Figueroa, & Melin, 2013). The device is reconfigurable such that a change to the system is easily achieved. Previous work has indicated that these devices provide a suitable platform for designing neuromorphic systems (Li, Cheung, Chan, Song, & Berger, 2013; Rice, Bhuiyan, Taha, Vutsinas, & Smith, 2009). Recently, some researchers have made full use of parallelism characteristics of FPGA to process neural signal and dramatically improved the computation speed. Arthur et al. (2012) fabricated a building block of a modular neuromorphic architecture using the FPGA as a simulation tool. This approach consists of 256 integrate-and-fire neurons and a 1,024_256 SRAM crossbar memory for synapses, so that the core is fully configurable in terms of neuron parameters, axon types, and synapse states. Wang et al. (2013) presented an FPGA implementation of a re-configurable, polychronous spiking neural network. They used a time multiplexing approach to implement 4096 (4k) neurons and up to 1.15 million programmable delay axons on a Virtex 6 FPGA. Bonabi, Asgharian, Safari, and Ahmadabadi (2014) presented efficient implementation of Hodgkin–Huxley-based (H–H) model of a neural network on FPGA. They employed different techniques such as sharing resources, CORDIC algorithm and can provide an opportunity to construct large FPGA-based network models to investigate the effect of different neurophysiological mechanisms. Indeed, trying to mimic biology, neuro-inspired systems have been extended in the recent years. High degree of parallelism and scalability makes this emerging computing technology especially interesting for real time applications.

The rest of this paper is organized as follows: In Section 2, the dynamic model of the astrocyte, the biological description of the Izhikevich neuron model, and its interaction with the astrocyte are covered. The digital circuits for neuron, astrocyte and the coupled neuron–astrocyte are described in Section 3. The MATLAB, ModelSim simulations and FPGA implementations are presented and discussed in Section 4. Finally, Section 5 concludes the paper.

2. Dynamic models of neuron and astrocyte

In this section, we first present the mathematical description of the astrocyte and then we explain the Izhikevich dynamic model of neuron.

2.1. The astrocyte model

Astrocytes, the dominant glial cell type, have become the focus of much attention in the past two decades. In addition to their roles in many of the supportive functions of the brain, new functions are beginning to emerge. Abundant evidence now supports the notion that astrocytes are actively involved in synaptic transmission in most brain regions (Halassa, Fellin, & Haydon, 2009; Volterra, Liaudet, & Savtchouk, 2014). Although astrocytes cannot elicit propagating action potentials (APs) like neurons do, their "unit of excitation" is the transient increase in intracellular calcium (Ca^{2+}) levels that is elicited by various neurotransmitters (e.g., glutamate, ATP, etc.). These astrocytic Ca^{2+} transients in turn lead to astrocytic release of transmitters (often referred to as "gliotransmitters") and to propagating Ca^{2+} waves (Di Castro et al., 2011; Giugliano, 2009; Newman, 2003). Astrocytes also communicate in a feedback mode with neurons. In response to elevated levels of intracellular Ca^{2+}, astrocytes can release gliotransmitters such as glutamate which bind to extrasynaptic receptors on the post synaptic neuron (Colangelo, Alberghina, & Papa, 2014; Corlew, Brasier, Feldman, & Philpot, 2008). This bidirectional communication between astrocytes and neurons indicates that astrocyte is a third signaling element at the "tripartite synapse" (Fellin, Pascual, & Haydon, 2006; Newman, 2003) that is shown in Fig. 1.

Postnov and colleagues introduced a mathematical model of the astrocyte that models the dynamics of the intracellular Ca^{2+} waves (Postnov, Koreshkov, Brazhe, Brazhe, & Sosnovtseva, 2009). This is a generalized and simplified mathematical model for a small neuron–astrocyte ensemble which considers the main pathways of bidirectional neuron–astrocyte signaling. Consequently, this model will be useful to study the main types of astrocyte response to neural activities and the resulting dynamical patterns and thereby, it will allow us to predict their changes with varying control parameters. This model is explained with the following set of equations (Postnov et al., 2009)

$$\tau_c \frac{dc}{dt} = -c - c_4 f(c, c_e) + (r + \beta S_m) \tag{1}$$

$$\varepsilon_c \tau_c \frac{dc_e}{dt} = f(c, c_e) \tag{2}$$

$$f(c, c_e) = c_1 \frac{c^2}{1 + c^2} - \left(\frac{c_e^2}{1 + c_e^2}\right)\left(\frac{c^4}{c_2^4 + c^4}\right) - c_3 c_e \tag{3}$$

$$\tau_{Sm} \frac{dS_m}{dt} = (1 + \tanh[S_{Sm}(z - h_{Sm})]) \times (1 - S_m) - \frac{S_m}{d_{Sm}} \tag{4}$$

$$\tau_{Gm} \frac{dG_m}{dt} = (1 + \tanh[S_{Gm}(c - h_{Gm})]) \times (1 - G_m) - \frac{G_m}{d_{Gm}}. \tag{5}$$

In these equations c and c_e are the calcium concentration in the astrocyte cytoplasm and within the endoplasmic reticulum, respectively. The calcium influx from the extracellular space is sensitive to the production of secondary messenger S_m (IP_3), which is controlled by the factor β. Interaction between cytoplasmic calcium and calcium in endoplasmic reticulum is defined by the nonlinear function $f(c, c_e)$. We set the control parameters r, β, τ_c, τ_{Sm}, τ_{Gm}, S_{sm}, S_{Gm}, h_{sm}, h_{Gm}, d_{sm}, d_{Gm}, ε_c to the values listed in Table 1. The values are taken from Amiri, Montaseri, and Bahrami (2011b); Amiri et al. (2012a); Postnov et al. (2009). As a result of augmentation of calcium concentration in the cytoplasm, astrocyte mediator G_m is released. The interaction between astrocyte and neuron is denoted with the parameter z (astrocyte input) that shows the synaptic activity of the neuron.

2.2. Neuron model

Izhikevich neuron model is a mathematical model that reproduces spiking and bursting behavior of known types of

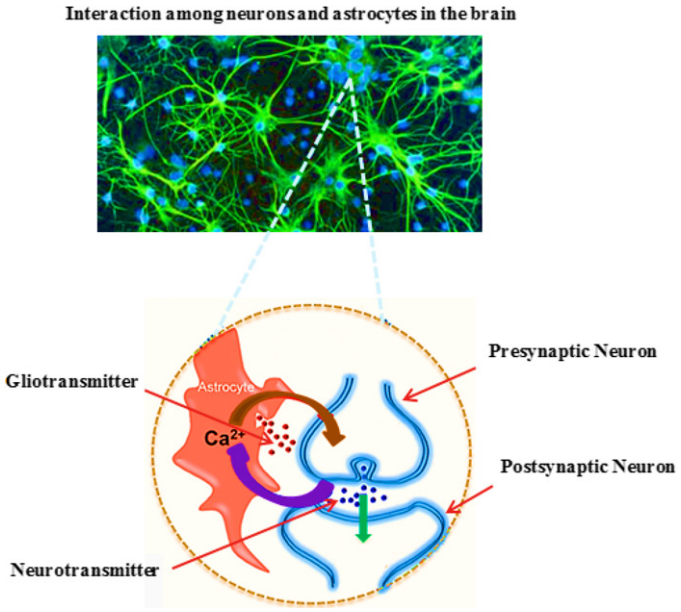

Fig. 1. The tripartite synapse in which astrocytes regulate the synaptic transmission via uptake of neurotransmitters or release of gliotransmitters spaces.

Table 1
Parameter values of neuron and astrocyte dynamical models used in the simulations.

Spiking behavior		Bursting behavior	
A	0.02	A	0.02
B	0.2	B	0.2
C	−65	C	−50
D	6	D	1.5
v_{th}	30	v_{th}	30
Astrocyte Parameters			
T_c	2	T_{sm}	10
c_1	0.13	d_{sm}	0.071
c_2	0.9	S_{sm}	100
c_3	0.004	h_{sm}	0.015
c_4	100	T_{Gm}	1.5
ε_c	0.01	d_{Gm}	2.5
r	0.02	S_{Gm}	100
β	1	h_{Gm}	0.025
θ_s	0.2	σ_s	0.02

cortical neurons. In this model, the dynamics of the membrane potential, v, is as follows: (Izhikevich, 2003)

$$v' = 0.04v^2 + 5v + 140 - u + I \tag{6}$$

$$u' = a(bv - u) \tag{7}$$

with the auxiliary after-spike resetting

$$\text{If } v \geq 30mv \begin{cases} v \leftarrow c \\ u \leftarrow u + d \end{cases} \tag{8}$$

where a, b, c, d are neuron parameters and their values are listed in Table 1. u is the membrane recovery variable, which accounts for the activation of K^+ ionic currents and inactivation of Na^+ ionic currents (Izhikevich, 2003). After the membrane voltage reaches +30 mV, the membrane voltage and the recovery variable are reset according to (8). The variable I is the input current.

2.3. Neuron–astrocyte interactions

Two-way communication between neuron and astrocyte is essential for axonal conduction, synaptic transmission, information processing and thus is required for normal functioning of the nervous system (Frühbeis, Fröhlich, & Krämer-Albers, 2012; Frühbeis et al., 2013). To develop a biologically inspired model and in order to clarify astrocyte dependent regulation of neural activities, astrocyte is connected to the neuron model. Brain function actually arises from the coordinated activity of a network comprising both neurons and glia (Perea, Navarrete, & Araque, 2009). Here we proceed in a phenomenological manner and utilized a functional approach to describe the loop of information exchange between neuron and astrocyte rather than a detailed biophysical and biochemical model (Amiri, Bahrami, & Janahmadi, 2011a, 2012c).

The relative number of astrocytes, expressed both as a proportion of total brain cell number and as a ratio to neuronal number, increases dramatically with phylogeny and brain complexity; on the other side, the relative expansion of astrocytes compared to neurons and more specifically, the relative predominance of astrocytes in the human brain cannot be readily explained (Nedergaard, Ransom, & Goldman, 2003). In the human frontal cortex, the ratio of glia to neurons is about 1.65 (Oberheim, Wang, Goldman, & Nedergaard, 2006). Given that astrocytes comprise about 50% of the total number of glial cells, a 1:1 ratio seems to characterize an acceptable approximation (Reato et al., 2012). The synaptic interactions are modeled in the same way as suggested by Terman, Rubin, Yew, and Wilson (2002). Generated action potential results in the release of neurotransmitter in which its concentration in synaptic cleft is modeled by the following equation:

$$[T] = \frac{1}{1 + \exp\left(-(v(t) - \theta_s)/\sigma_s\right)} \tag{9}$$

where θ_s and σ_s are the half-activation voltage and steepness of the sigmoid function, respectively. It is now well-documented that astrocytic neurotransmitter receptors can be activated by synaptic neurotransmitters released by neuron, that is $[T]$. Following Volman, Ben-Jacob, and Levine (2007), we assume that the rate of IP_3 production depends on the concentration of neurotransmitter which is released to the synaptic cleft. Therefore, the input of the astrocyte (z) which triggers the production of IP_3, is defined as:

$$z = \lambda [T] \tag{10}$$

where $\lambda > 0$ is an amplifying parameter. Astrocytes with a physiological feedback can respond to synaptic neurotransmitters in brain and participate in synaptic signaling. This gives increase in depolarization or hyperpolarization of nearby neurons (Smith,

Table 2
Comparison between LUT and LAM in hardware implementation.

Required number of	tanh(·)		$\frac{x^2}{1+x^2}$		$\frac{1}{\left(1+\exp\left(\frac{v[n]-\theta_S}{\sigma_S}\right)\right)}$		v-nullcline	
	LUT	LAM	LUT	LAM	LUT	LAM	LUT	LAM
Registers	35	8	33	8	8	5	23	4
Comparators	12	6	14	5	3	2	15	2
RMSE	0.0473	0.0304	0.0401	0.0233	0.000314	0.0002017	1.513	0.9905

2010). Specifically, astrocytic glutamate release in the hippocampus can activate NMDA (N-methyl-D-aspartate) type glutamate receptors, leading to so-called slow inward currents (SIC) in neighboring neurons (Fellin, 2009; Min, Santello, & Nevian, 2012). Consequently, the output of the astrocyte is modeled as Amiri, Montaseri, and Bahrami (2013b):

$$i^{ast} = \gamma \cdot G_m, \tag{11}$$

where γ is the feedback strength from astrocyte to neuron. Thus, the input current equation into the neuron with considering the effect of astrocyte feedback is modified as follows:

$$i\,(t) = i^{const}\,(t) + i^{ast}(t). \tag{12}$$

3. Hardware implementation

FPGA consists of thousands of reconfigurable logic elements. The wiring that connects logic elements is electrically reconfigurable. Therefore, components can be wired together to create one design. Then it can be erased and wired together differently to create a new one. Analog circuits are sensitive to fabrication process and VLSI implementation cannot be reconfigured easily; on the other hand, since FPGA is a digital device that owns reprogrammable properties and robust flexibility, many researchers have made great efforts on designing neuromorphic systems using FPGA technique (Li et al., 2013; Majumder, Pande, & Kalyanaraman, 2014).

In this section, we present a digital neuron–astrocyte circuit with a new architecture based on piecewise-linear approximation of the Izhikevich neuron model and Postnov astrocyte model. The general architecture is shown in Fig. 2. We consider the important criteria from the hardware point of view such as scaling up the designed circuit, reducing the digital implementation cost and keeping low power operation while obtaining results similar to the biophysical model of neuron–astrocyte interaction. Since a multiplier is an expensive block in terms of area and power consumption, in this research, we try to utilize simple blocks such as shifters and adders. This approach can help to reimburse the limited number of available fast multipliers on the chip and hence it is possible to implement large scale networks on low-cost and widely available hardware platforms such as FPGAs. The sequential approach is used and the output is produced in the last cycle of each iteration. For digital implementation of the neuron–astrocyte signaling, Single Constant Multiply (SCM) technique is used for efficient low-cost hardware implementation on digital platforms which change the multiplication of two variables to multiplication of one variable by a constant value.

One of the main challenges in digital implementation of the neuron and astrocyte dynamic model is the presence of nonlinear *nullclines*. One method is to use a look-up table (LUT) to approximate nonlinear functions which needs many comparators and several registers for memory space and therefore reduces the speed. In order to deal with these problems, we use linear approximation method (LAM) and try to approximate the nullclines of the astrocyte–neuron dynamical system with several line segments which decreases the implementation cost significantly (compared to the

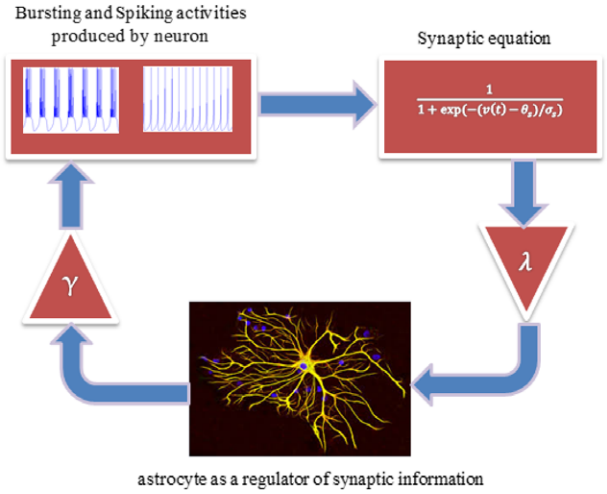

Fig. 2. The general architecture for hardware implementation.

original functions). Comparison between LAM and LUT for hardware implementation of different nonlinear functions is summarized in Table 2. In LAM, nonlinear functions will be replaced by first order functions. This approach provides some degrees of freedom to have a linear system with similar dynamics to the original nonlinear model. For approximating the v-nullcline of the neuron membrane potential, nonlinear nullclines in the form of $\tanh(\cdot)$, $\frac{x^2}{1+x^2}$, $\frac{x^4}{c_2^4+x^4}$ and $\frac{1}{\left(1+\exp\left(\frac{v[n]-\theta_S}{\sigma_S}\right)\right)}$ with several line segments, we used an exhaustive search algorithm. In this process, we started with a three-piece linear function. In other words, first, we selected two arbitrary points on the nonlinear curve to have three intervals. In each interval, the least squares method was used to fit linear equations on the original nonlinear curve. Next, we compute root-mean square error (RMSE) between piecewise-linear approximation and original nonlinear curve. We applied an exhaustive search approach and changed the position of two initial points to find the minimum RMSE, and then determined the coefficients of piecewise-linear function. The aforementioned process has been repeated from 2 to 6 initial points on nonlinear curve. After obtaining an RMSE lower than 0.05, the searching algorithm will be terminated. The results show that the considered error threshold is appropriate because the designed hardware can mimic the behavior of the biophysical neuron–astrocyte model (see the next section).

Fig. 3 shows the original and line approximation of the v-nullcline. It should be mentioned that u-nullcline is linear and thus no linear approximation is needed. Using parameter values listed in Table 1, the v- and u-nullclines can be obtained as follows:

$$\dot{v} = 0 \rightarrow 0.04v^2 + 5v + 140 - u = 0 \quad (v\text{-nullcline}) \tag{13}$$

$$u^{\cdot} = 0 \rightarrow 0.02\,(0.2v - u) = 0 \quad (u\text{-nullcline}). \tag{14}$$

Fig. 3(a) shows the v- and u-nullclines in blue and green, respectively. The intersections of the v- and u-nullclines are the *equilibrium* points which are depicted by red circles in Fig. 3. The equilibrium points are: $p_1(-50, -10), p_2(-70, -14)$. By

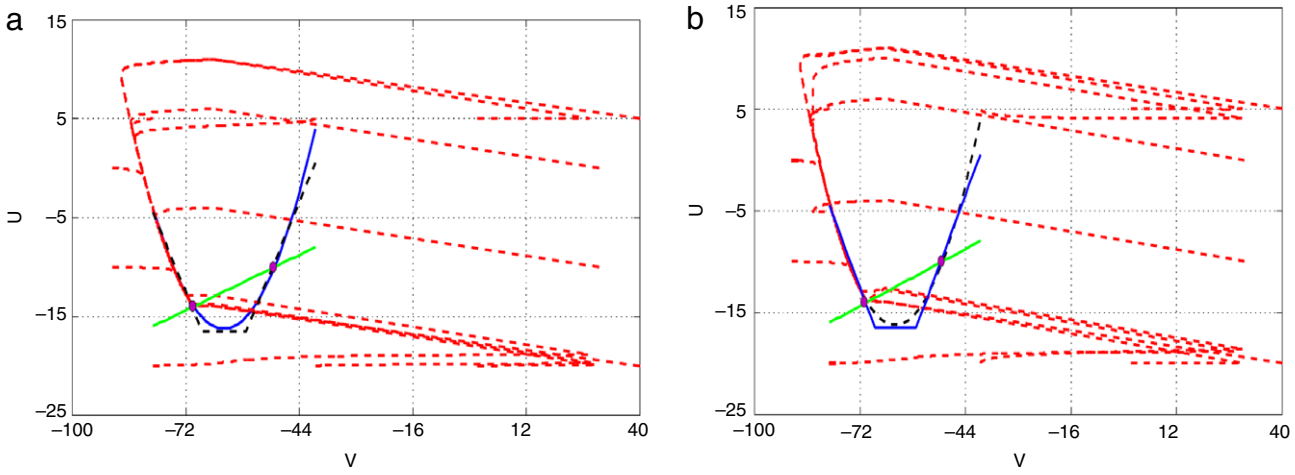

Fig. 3. (a) The original phase plane of the Izhikevich neuron. The blue curve is the original v-nullcline and the dashed black lines represent piecewise linear approximation. The green line is u-nullcline which is originally linear. The equilibrium points are shown by red circles. (b) The line segment approximation (blue lines) for the v-nullcline (dashed black curve). (For interpretation of the references to color in this figure legend, the reader is referred to the web version of this article.)

computing the Jacobian matrix at these equilibrium points, the eigenvalues can be obtained. Thus, for $p1$, we have: $\lambda = -0.4 \pm 0.8i$ which means that the p_1 is a stable focus and for p_2 we obtain $\lambda = -1.378$ and $\lambda = 0.579$ which is a saddle point. The trajectories plotted in Fig. 3 show the behavior of the system.

Considering, Fig. 3(b), the piecewise linear model can be obtained as follows (Soleimani, Ahmadi, & Bavandpour, 2012):

$$\dot{v} = 0.5 * |v + 68| + 0.5 * |v + 57| - 22 - u + I \quad (15)$$

$$\dot{u} = 0.02(0.2v - u). \quad (16)$$

Similarly, the equilibrium points of the approximated system are: $\tilde{p}_1(-50.625, -10.125)$, and $\tilde{p}_2(-70.415, -14.083)$ and therefore for $\tilde{p}1$, we have: $\lambda = -0.4 \pm 0.8i$ which means that the $\tilde{p}1$ is a stable focus and for $\tilde{p}2$ we obtain $\lambda = -1.566$ and $\lambda = 0.766$ which is a saddle point. Comparing the results of the stability analysis of the original Izhikevich neuron with its piecewise linear approximation model, it is evident that the dynamical characteristics of the original nonlinear system is preserved by its linear approximated model. Next, the piecewise linear model, Eqs. (15)–(16), are discretized using Euler method which is simple and produces acceptable responses that discretizing step (h) in our design is set to 0.015625. The discrete equations are as follows:

$$v[n+1] = (0.5 * |v[n] + 68| + 0.5 * |v[n] + 57| - 22 - u[n] + I)\, h + v[n] \quad (17)$$

$$u[n+1] = (0.02\,(0.2v[n] - u[n]))\, h + u[n]. \quad (18)$$

Next, we recruit the SCM technique and modify the coefficient constants so that they can be rewritten based on the power of 2. In this way, it is possible to replace the multiplication with shift and add operations. For example, the discretizing step (h) in our design is set to $0.015625 = 1/64 = 1/(2^6)$ and can be implemented by six arithmetic shifts to the right. It should be emphasized that this structure can be optimized in area and speed through pipelining and resource sharing. The modified parameters are listed in Table 3. Since in our design, only one multiplier is used, the minimum clock pulse period should be equal to the minimum required time for multiply operation. However, fewer states are required to produce the output compared to the original model. For example in the conventional method to perform $a * dt$, two states are required and the output is produced in the third state. Nevertheless, utilizing the shift operation, only one state is needed and the output is produced in the second state.

Table 3
Modified parameter values of neuron and astrocyte dynamical models used in the digital implementation.

Spiking behavior		Bursting behavior	
A	0.02	A	0.03125
B	0.2	B	0.25
C	−65	C	−50
D	6	D	1.5
v_{th}	30	v_{th}	30
Astrocyte parameters			
T_c	2	T_{sm}	10
c_1	0.125	d_{sm}	0.071
c_2	1	S_{sm}	128
c_3	0.0039	h_{sm}	0.5
c_4	128	T_{Gm}	1.5
ε_c	0.015625	d_{Gm}	2.5
r	0.02	S_{Gm}	128
β	1	h_{Gm}	0.025
θ_s	0.25	σ_s	0.03125

Each desired signal can be converted to analog signal using digital-to-analog converter chip. In this work, we used VGA support on the ZedBoard development kit. Fig. 4 describes the necessary steps to generate the membrane potential (v) and the recovery variable (u) of the neuron in iteration. This process is performed for producing each output sample using last samples. In our digital implementation, a memory register is used at each output block. It stores the outputs which will be used in the next calculations. Individual state variables are solved in n-bits registers which can be determined based on the required precision for implementation and type of application. In our research, $n = 20$ (4 bits for integer part and 16 bits for fractional part). Since c_e dynamic has very small value, 16 bits are required for fractional part in fixed-point calculations to reproduce its dynamics on hardware appropriately.

Similarly, the dynamical equations of astrocyte model are discretized using Euler method. The discretizing step (h) in our design is set to 0.015625. The discrete equations are as follows:

$$c[n+1] = \left(-c[n] - c_4\left(c_1 \frac{c[n]^2}{1 + c[n]^2} - \left(\frac{c_e[n]^2}{1 + c_e[n]^2}\right)\left(\frac{c[n]^4}{c_2^4 + c[n]^4}\right) - c_3 c_e[n]\right) + r + \beta s_m[n]\right)\frac{h}{\tau_c} + c[n] \quad (19)$$

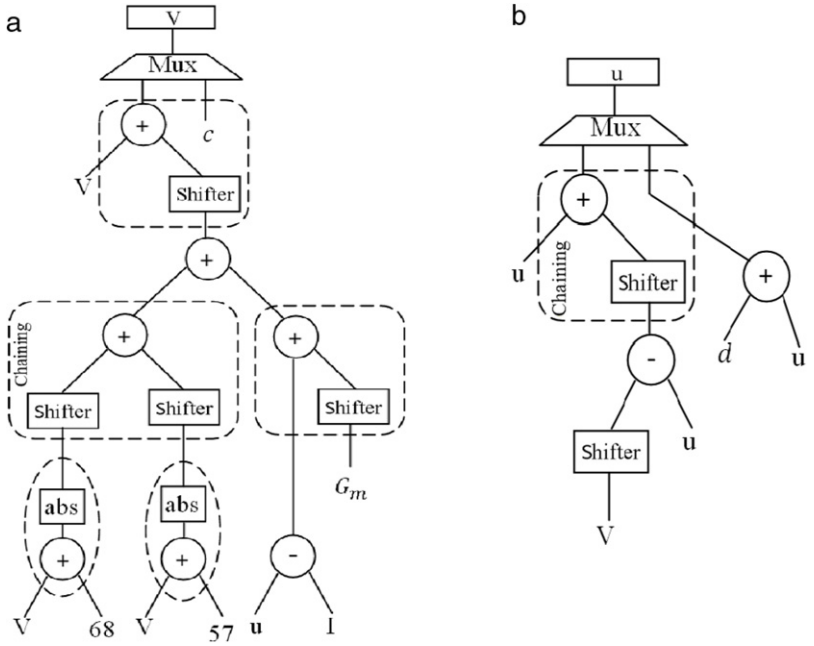

Fig. 4. Scheduling diagram for (a) membrane potential (v dynamic) and (b) the membrane recovery variable (u dynamic).

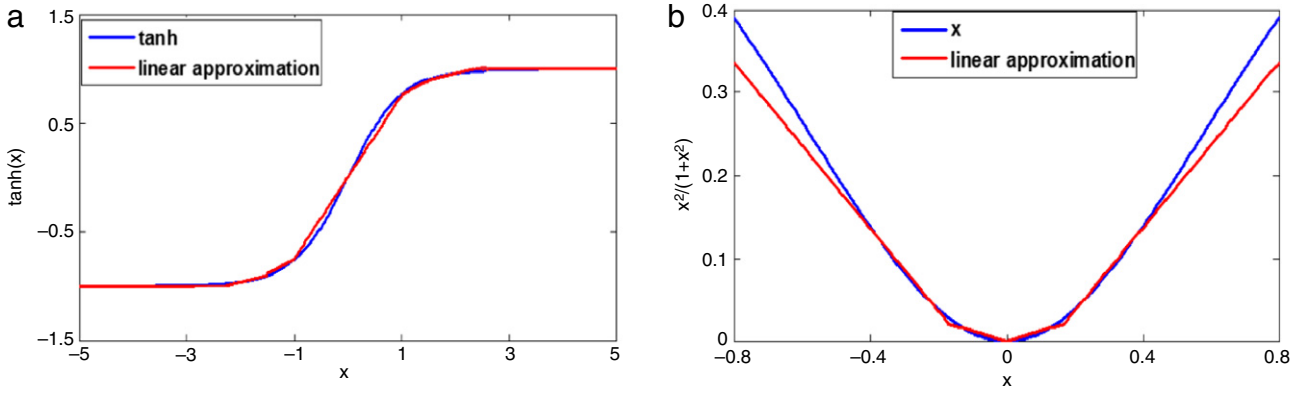

Fig. 5. (a) 7-line segments approximation for the tanh function, (b) 6-line segments approximation for the $\frac{x^2}{1+x^2}$ function.

$$c_e[n] = \left(c_1\frac{c[n]^2}{1+c[n]^2} - \left(\frac{c_e[n]^2}{1+c_e[n]^2}\right)\left(\frac{c[n]^4}{c_2^4+c[n]^4}\right) - c_3c_e[n]\right) \times \frac{h}{\varepsilon_c\tau_c} + c_e[n+1] \tag{20}$$

$$s_m[n+1] = \left[\left(1+\tanh\left(s_{sm}\left(\frac{1}{\left(1+\exp\left(\frac{v[n]-\theta_s}{\sigma_s}\right)\right)} - h_{sm}\right)\right)\right) \times (1-s_m[n]) - \frac{s_m[n]}{ds_m}\right]\frac{h}{\tau_{sm}} + s_m[n] \tag{21}$$

$$G_m[n+1] = \left[(1+\tanh(s_{Gm}(c[n]-h_{Gm}))) \times (1-G_m[n]) - \frac{G_m[n]}{dG_m}\right]\frac{h}{\tau_{Gm}} + G_m[n]. \tag{22}$$

Similar to the procedure used for neuron circuit, the linear approximation method is utilized and the nullclines of the dynamical system is approximated with several line segments. Fig. 5 shows the line approximation of the tanh(·), $\frac{x^2}{1+x^2}$ functions so that it preserves the dynamical characteristics of the original nonlinear system. As previously discussed, an exhaustive search algorithm is utilized to find the best parameter values of the line segments which lead to the minimum RMSE.

The coefficient constants are determined using power of 2 which in turn make it possible to use shift operation instead of multiplication. Considering, circuit complexity (required number of adders, multipliers, comparators) and the required computational accuracy, the 7-line and 6-line segments approximation were used for tanh(·) and $\frac{x^2}{1+x^2}$ functions respectively. The parameter values of the resulted lines are listed in Tables 4 and 5. The RMSE is 0.0304 and 0.0233 for tanh and $\frac{x^2}{1+x^2}$ line approximations, respectively.

Also 3-line segments approximation is used for $\frac{1}{(1+\exp\left(\frac{0.2-v}{0.02}\right))}$ function, with good precision as illustrated in Fig. 6. The RMSE is 0.0002017 for this approximation. The parameter values of the resulted lines are listed in Table 6. This leads to the elimination of using multiplier for digital circuit of synapse.

We try to use the minimum required resources to design the digital circuit to reduce the digital implementation cost. In this way, for the approximation of the $\frac{c^4}{c_2^4+c^4}$ function, considering $c^2 = x$, we can use $\frac{x^2}{1+x^2}$ function which already has been approximated

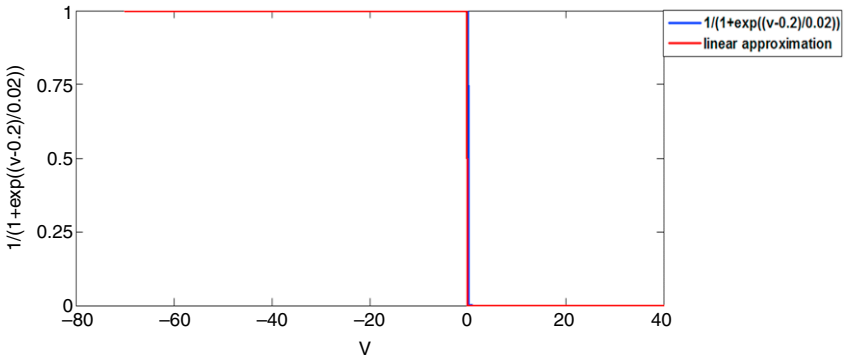

Fig. 6. Approximation of the sigmoid function of the synapse with 3-line segments approximation. In this way, there is no need to use multiplier for digital circuit of synapse.

Table 4
The parameter values of individual lines for the 7-line segments approximation of the $\tanh(x)$ with $A_1^* x + B_1$.

Region of X	A_1	B_1
$X > 2.5$	0	1
$1.5 =< X <= 2.5$	0.125	0.7150148
$1 < X < 1.5$	0.25	0.5115941
$-1 =< X <= 1$	0.75	0
$-1.5 < X < -1$	0.25	−0.5115941
$-2.5 =< X <= -1.5$	0.125	−0.7150148
$X < -2.5$	0	−1

Table 5
The parameter values of individual lines for the 6-line segments approximation of the $\frac{x^2}{1+x^2}$ with $A_2^* x + B_2$.

Region of X	A_2	B_2
$X > 0.8$	0.5	−0.06375
$0.17 =< X <= 0.8$	0.5	−0.06375
$0 < X < 0.17$	0.125	0
$-0.17 =< X <= 0$	−0.125	0
$-0.8 < X < -0.17$	−0.5	−0.06375
$X <= -0.8$	−0.5	−0.06375

Table 6
The parameter values of individual lines for the 3-line segments approximation of the $\frac{1}{(1+\exp\left(\frac{0.2-v}{0.02}\right))}$ with $A^* x + B$.

Region of X	A	B
$X > 0.3$	1	0
$0.3 =< X <= 0.1$	5	−0.4866
$X < 0.1$	0	0

with 6-line segments. Therefore, the discrete equations for the linear approximation of the astrocyte dynamic model are described by:

$$c[n+1] = \big(-c[n] - c_4(c_1(A_2 * c[n] + B_2) - (A_2 * c_e[n] + B_2)(A_2 * c[n] * c[n] + B_2) - c_3 c_e[n]) + r + \beta s_m[n]\big)\frac{h}{\tau_c} + c[n] \quad (23)$$

$$c_e[n] = \big(c_1(A_2 * c[n] + B_2) - (A_2 * c_e[n] + B_2) \times (A_2 * c[n] * c[n] + B_2) - c_3 c_e[n]\big)\frac{h}{\varepsilon_c \tau_c} + c_e[n+1] \quad (24)$$

$$s_m[n+1] = \Big[(1 + A_1 * (s_{sm}((A_3) - h_{sm})) + B_1) \times (1 - s_m[n]) - \frac{s_m[n]}{ds_m}\Big]\frac{h}{\tau_{sm}} + s_m[n] \quad (25)$$

Table 7
Low-level device utilization summary.

Slice logic utilization	Used	Available	Utilization
Number of slice LUTs	1349	53,200	2%
Number of bonded IOBs	9	200	4%
Number of slice registers	853	106,400	1%

Table 8
High-level device utilization summary.

Synthesis report	
$20 * 20$-bit multipliers	1
20-bit adder	5
20-bit subtractors	6
Flip-flops	923
Comparators	15
Multiplexers	132
FSMs	1

$$G_m[n+1] = \Big[(1 + A_1 * (s_{Gm}(c[n] - h_{Gm})) + B_1) \times (1 - G_m[n]) - \frac{G_m[n]}{dG_m}\Big]\frac{h}{\tau_{Gm}} + G_m[n]. \quad (26)$$

Considering Z as the input and G_m as the output, the scheduling diagrams for each discrete equation is shown in Fig. 7. Similar to the neuron circuit, at each block output, there is a memory register to store the outputs to be used in the next calculations. Indeed, the input is applied to the approximation unit and then based on the input region and Tables 4–6, the appropriate A_i and B_i are selected. They will be updated with new states after completion of iteration. Considering the minimum precision required for the digital implementation of the C, C_e, S_m and G_m dynamics, 20 bits are used.

The data type used in FPGA implementation is single fixed point (20-bits: 4 bits for integer part and 16 bits for fractional part). First, we simulated the neuron–astrocyte dynamical system in MATLAB and obtained the range of variable's fluctuations. Next, the required accuracy has been determined using this range of fluctuations. Finally, for FPGA implementation, fractional and integer parts were used to achieve required accuracy utilizing fixed-point calculations. In this way, using floating point calculations in MATLAB we could reach the simpler fixed-point calculations in hardware.

With efficient use of the 20-bit registers in our design, the digital neuron–astrocyte circuit was simulated and synthesized using Verilog and Xilinx ISE tools, respectively, resulting 1% utilization and a maximum clock frequency of 276 MHz. The resource utilization of the FPGA implementations is summarized in Tables 7 and 8.

4. Results of simulations and hardware implementation

The network shown in Fig. 2 illustrates the configuration we used for this experiment. In this section, the results of

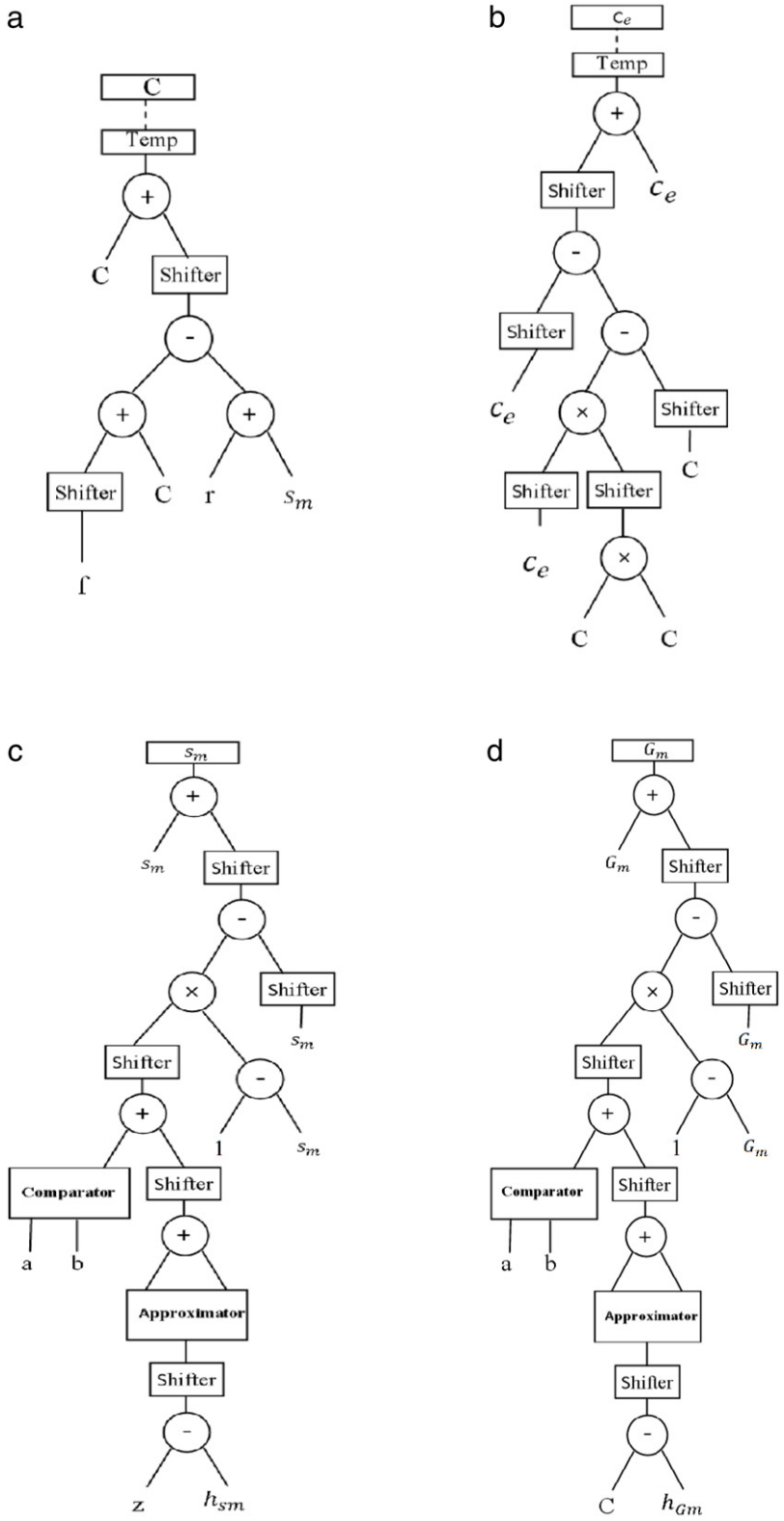

Fig. 7. Scheduling diagram for (a) calcium concentration in the astrocyte cytoplasm, c, (b) calcium concentration within the endoplasmic reticulum, c_e (c) the second messenger IP_3, S_m (d) astrocyte output, G_m.

software simulations and hardware implementation of the neuron–astrocyte crosstalk are presented.

We discuss how the digital astrocyte–neuron circuit can produce the similar response such as its biological counterpart in different conditions. In the following, we design four experiments to show the flexibility and ability of the designed circuit in mimicking the behavior of biological neuron–astrocyte model. To consider a wide range of behaviors, both spiking and bursting activities are selected. Model parameters for spiking and bursting activities are listed in Tables 1 and 3.

In the first experiment we open the astrocyte feedback (i.e., $\gamma = 0$). Fig. 8(a) and (b) shows the neuron membrane voltage

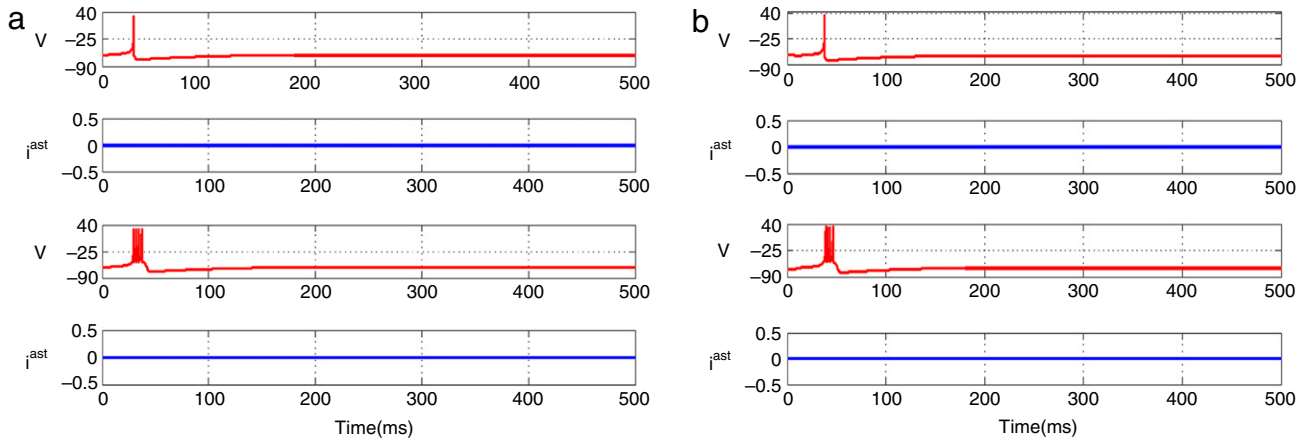

Fig. 8. The time response of the neuron (v) in mv and the astrocyte output (i^{ast}) in μA for (a) MATLAB simulations of the original model of neuron–astrocyte interaction and (b) VHDL simulation of the designed digital circuit. In these simulations $\lambda = 0.5$ and $\gamma = 0$, the first and the third panels show the single spike and burst activities of the neuron respectively. The second and the fourth panels are the astrocyte output current which is zero since $\gamma = 0$.

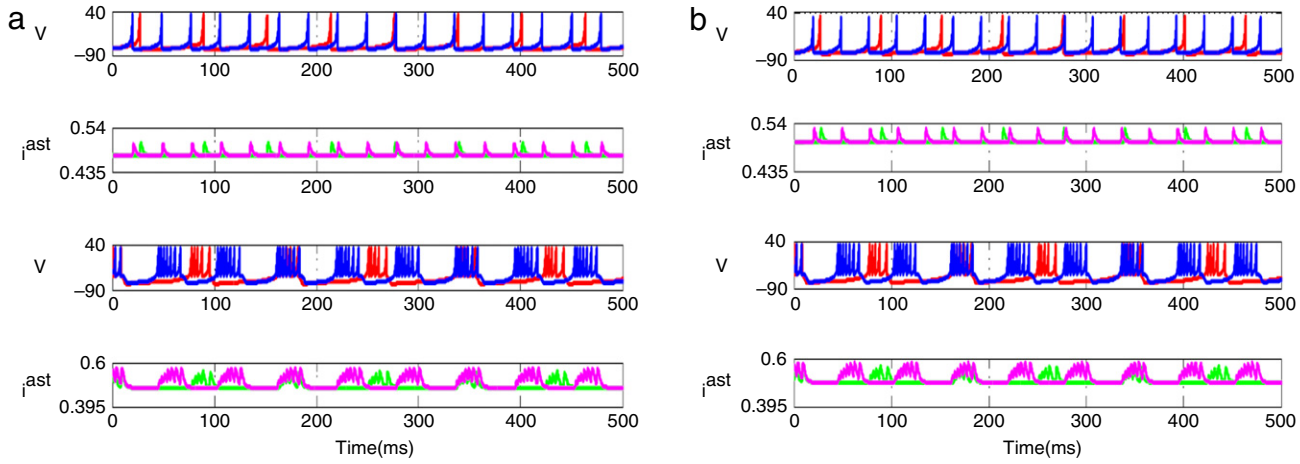

Fig. 9. The time response of the neuron (v) in mv and the astrocyte output (i^{ast}) in μA for (a) MATLAB simulations of the original model of neuron–astrocyte interaction and (b) VHDL simulation of the designed digital circuit. The first and the third panels show the spiking and bursting activities of the neuron, respectively. The second and the fourth panels show the astrocyte output current corresponds to the neuron spiking and bursting activities, respectively. In these simulations when $\lambda = 0.5$ and $\gamma = 1$, neuron membrane potential and astrocyte output current show with red and green color respectively and with selecting $\lambda = 0.5$ and $\gamma = 5$, neuron membrane potential and astrocyte output current show with blue and pink color respectively. It is evident that increasing the feedback strength from astrocyte to neuron, first activates the silent neuron and then increases its firing frequency. (For interpretation of the references to color in this figure legend, the reader is referred to the web version of this article.)

and the astrocyte current for the MATLAB simulations of the original neuron–astrocyte model and ModelSim simulations of its digital circuit, respectively. According to Fig. 8, only a single action potential or burst could be observed and thus the digital model is clearly capable of working in both spiking and bursting behaviors of biological neurons.

Next, we consider the more realistic situation and consider the role of astrocyte in the regulation of synaptic transmissions. So, for this experiment, the configuration in Fig. 2 is being used with $\lambda = 0.5$ and $\gamma = 1$ (neuron activity with blue and astrocyte output current with green in Fig. 9) and this configuration is considered with $\lambda = 0.5$ and $\gamma = 5$ (neuron activity with red and astrocyte output current with pink in Fig. 9). As shown in Fig. 9, when we consider the close-loop astrocyte feedback, the neural firing rate is increased. Fig. 9(a) shows the neuron membrane voltage and the astrocyte current for spiking and bursting activities obtained by MATLAB simulations of the original neuron–astrocyte model and Fig. 9(b) shows the neuron membrane voltage and the astrocyte current for spiking and bursting activities obtained by ModelSim simulation of its relevant digital circuit. As depicted in Fig. 9, with considering the role of astrocyte in synaptic activity and increase the feedback strength from astrocyte to neuron, first the silent neighboring neuron can be turned on and generates spikes or bursts and then increases its firing frequency.

In order to indicate the precision of the designed digital circuit, the RMSEs between VHDL and MATLAB simulation results are listed in Table 9.

By comparing the simulation results shown in Figs. 8 and 9 together, we will conclude that the firing frequency of the neuron is significantly increased as the astrocyte feedback strength is increased from 1 to 5. Therefore, the astrocyte affects neuronal excitability by providing feedback mechanism. In this way, astrocyte is able to change the neuron spiking frequency or turn on the silent neuron which in turn leads to the emergence of different neural responses. On the other hand, based on different neural coding schemes, the firing pattern of a neuron, which includes both the frequency and the timing of action potentials, is a key component of information processing in the brain. In the "temporal code", the precise timing of action potentials is important and in the "rate code", the information is represented by a modulation of the firing rate (Quilichini & Bernard, 2012). In this way, it was demonstrated that the astrocyte could apply feedback mechanism to regulate neuronal excitability. Thus, variation in the strength of astrocyte–neuron interactions can be considered as a mechanism

Table 9
The RMSE between VHDL and MATLAB simulations.

	$\gamma = 0$		$\gamma = 1$		$\gamma = 5$	
	Spiking mode	Bursting mode	Spiking mode	Bursting mode	Spiking mode	Bursting mode
V	0.412	0.364	1.01	0.5	2.13	1.752
i^{ast}	0	0	0.0261	0.0703	0.041	0.0842

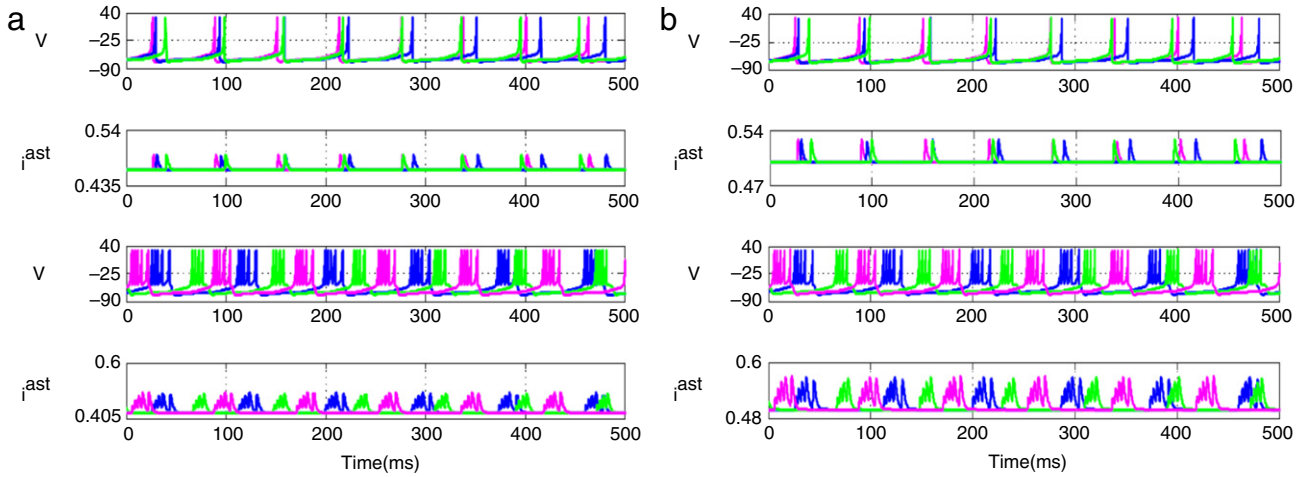

Fig. 10. The time response of the neuron (v) in mv and the astrocyte output (i^{ast}) in μA for (a) MATLAB simulations of the original model of neuron–astrocyte interaction and (b) VHDL simulation of the designed digital circuit. The first and the third panels show the spiking and bursting activities of the neuron respectively. The second and the fourth panels show the astrocyte output corresponds to the neuron spiking and bursting activities, respectively. In these simulations γ was fixed at $\gamma = 1$ and λ was changed and took on three different values of (a)$\lambda = 0.5$ (blue, spiking: T = 132.98 ms, bursting: T = 144.3 ms) $\lambda = 0.6$ (pink, spiking: T = 130.31 ms, bursting: T = 141.62 ms) and $\lambda = 0.7$ (green, spiking: T = 128.03 ms, bursting: T = 139.46 ms). (b) $\lambda = 0.5$ (blue, spiking: T = 64.6 ms, bursting: T = 86.9 ms) $\lambda = 0.6$ (pink, spiking: T = 62.65 ms, bursting: T = 82.4 ms) and $\lambda = 0.7$ (green, spiking: T = 59.41 ms, bursting: T = 80.9 ms). It is evident that increasing λ, the firing frequency of the neuron will increase. (For interpretation of the references to color in this figure legend, the reader is referred to the web version of this article.)

for information encoding. Indeed, the astrocyte is capable to regulate the synaptic transmission via uptake of neurotransmitters or release chemical transmitters into synaptic space and thus, the neuron–astrocyte interaction can facilitate the diversity of responses produced by the neuron. In line with these simulation results, recent studies about communications between astrocytes and neurons reveal that glutamate release from single astrocyte may control the excitability of neighboring cells (Silchenko & Tass, 2008), that is, the astrocytes can act as local controllers of the synaptic function (Fellin, 2009; Fellin et al., 2006). Our preliminary simulations therefore show that the output of the proposed digital neuron–astrocyte circuit is in good agreement with the original dynamic model in different conditions. In addition, the low RSME values validate the circuit performance.

To reveal the ability of proposed digital neuron–astrocyte circuit in mimicking the behavior of the biophysical counterpart, we perform the third experiment. In this experiment, we consider the effect of variation of λ (neuron to astrocyte feed-forward strength) in Eq. (10). To understand the effect of this changing, in Fig. 10, we changed value of λ from 0.5 to 0.7 and fixed $\gamma = 1$. Clearly, it can be visible that changing λ from 0.5 (blue curve) to 0.6 (pink curve) and finally to 0.7 (green curve) increases firing frequency of the neuron. So, variation in neuron to astrocyte feed-forward strength can affect neuron excitability and finally information encoding mechanism. The time responses of the neuron and astrocyte outputs for the MATLAB simulations of the original neuron–astrocyte model and ModelSim simulations of the digital circuit are shown in Fig. 10(a) and (b), respectively. To investigate the effect of changing λ and γ on the neuronal behavior simultaneously, we calculated the neuron spiking frequency (that is the inverse on inter-spike intervals) and then plotted it versus λ and γ. The result for digital neuron–astrocyte circuit is shown in Fig. 11. The color shows spiking frequency of the digital neuron. As can be observed, for large value of λ and γ, the frequency is increased considerably. Two important results are derived from this figure. First, we observe a transition in the digital neuron firing frequency as the strength of the neuron–astrocyte interactions changes. Second, the locus of the constant frequency points suggests that there is a nonlinear relationship between the feed-forward (from neuron to astrocyte) and feedback (from astrocyte to neuron) gains in the neuron–astrocyte communication. In this way, to have a specific firing activity, the interaction of both parameters is required which reveal the fundamental role of the digital astrocyte to regulate the neural excitability.

It was demonstrated that function of the designed circuit is compatible with that of the neuron–astrocyte model with diversity similar to that of biological model. The circuit provides a simple, compact and easy configurable universal digital circuit of neuron–astrocyte interaction. Clearly, using the new architecture increased the hardware resources but contributed to the adaptability of neural responses.

To evaluate the performance of the digital circuit in hardware, it has been implemented on the ZedBoard development kit. The expandability features of this evaluation and development platform make it ideal for rapid prototyping and proof-of-concept development. The primary objective is to examine the feasibility of FPGA implementation of the model and to show that hardware can reproduce the model responses. The system is developed under the Xilinx ISE 14 Foundation Design Software Environment using Verilog HDL.

Fig. 12 displays oscilloscope photographs of the digital implementation of the neuron–astrocyte interactions. In this figure, the output of the FPGA board was shown in yellow (membrane voltage) and blue (astrocyte output current) colors, respectively. Fig. 12(a) shows the spiking behavior and Fig. 12(b) illustrates the bursting activates. It should be mentioned that we use the digital to analog converter, build in the ZedBoard. The FPGA experiments

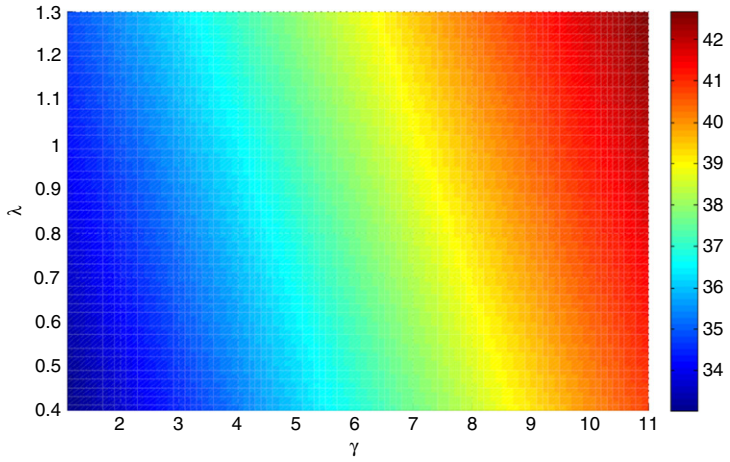

Fig. 11. The result of Verilog simulations of the neuron–astrocyte digital circuit to investigate the effect of bidirectional communication between neuron and astrocyte on the neuronal behavior. The neuron firing frequency is plotted as a function of λ and γ with different colors. (For interpretation of the references to color in this figure legend, the reader is referred to the web version of this article.)

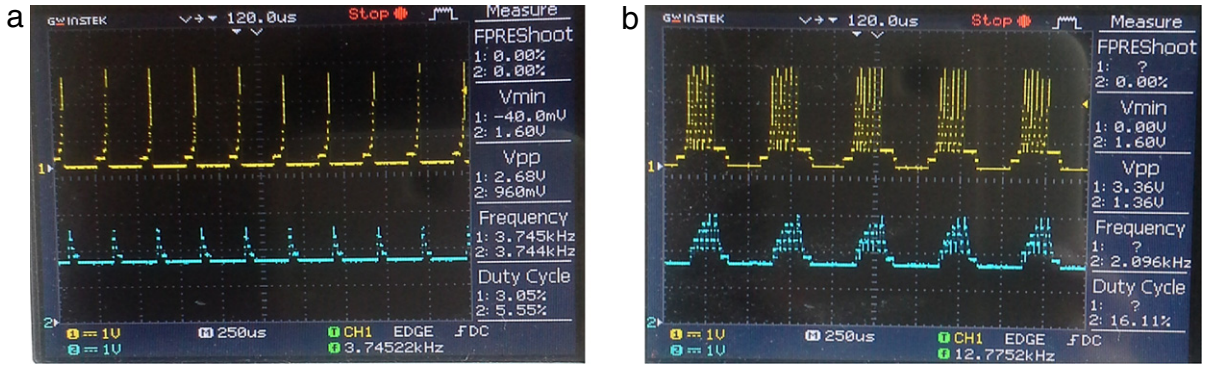

Fig. 12. The results of hardware implementation of the designed digital circuit for the neuron–astrocyte communication on the ZedBoard development kit. The membrane voltage and the astrocyte output are shown in yellow and blue, respectively using D/A converter. (a) The spiking behavior. (b) The bursting activity. The Time and Volt divisions of the oscilloscope are set on 250 us for (a), (b) and 1V for (a), (b), respectively. It is obvious that the hardware behavior shows neuron–astrocyte signaling.

show that the digital implementation of neuron–astrocyte communication reproduces nonlinear responses of the biological counterpart, where the general-purpose FPGA is used to provide fundamental experimental results for developing a future physical-level design.

5. Conclusion

Understanding the computational principles used by the brain and how they are physically embodied is crucial for developing novel computing paradigms. This guides a new generation of technologies that can combine the strengths of industrial scale electronics with the computational performance of brains. Neuronal firing activity, which includes both the frequency and the timing of action potentials, is an essential component in information processing in the brain (Quilichini & Bernard, 2012). In addition, over the past decade, the knowledge about the diverse role of astrocytes in many facets of synaptic transmission has considerably expanded (Rusakov, Zheng, & Henneberger, 2011). In order to exploit the principal advantages of using FPGA such as fast prototyping and ease of implementation, the present study puts forward a new perspective to analyze the process of bidirectional information exchange between the neuron and astrocyte from a hardware viewpoint. Considering the results of this paper which implies that the digital astrocyte is able to change the neuron spiking frequency, suggests that the digital astrocyte could also be used as an active element in neuromorphic applications.

In this paper, we explored the feasibility of using FPGAs for implementing neuron–astrocyte interactions. The results of the FPGA implementation were in agreement with those of ModelSim and MATLAB simulations and showed that a digital astrocyte–neuron circuit might be utilized in brain like computing systems. In this way, we proposed a digital neuron–astrocyte model suitable for development of spiking neural networks on FPGAs aiming at flexibility, parallelism and bio-plausibility, while having hardware implementation in mind.

While modulation of the synaptic transmission by astrocytic mechanisms was demonstrated in hardware, it was only a first step in digital circuits to implement the complex interactions between neurons and astrocytes. Future works aim to extend this model to form the tripartite synapse. It should be noted that the role of glial cells in neural activity and information processing in brain is not completely understood.

References

Ambroise, M., Levi, T., Joucla, S., Yvert, B., & Saïghi, S. (2013). Real-time biomimetic Central Pattern Generators in an FPGA for hybrid experiments. *Frontiers in Neuroscience*, *7*.

Amiri, M., Bahrami, F., & Janahmadi, M. (2011a). Functional modeling of astrocytes in epilepsy: a feedback system perspective. *Neural Computing and Applications*, *20*(8), 1131–1139.

Amiri, M., Montaseri, G., & Bahrami, F. (2011b). On the role of astrocytes in synchronization of two coupled neurons: a mathematical perspective. *Biological Cybernetics*, *105*(2), 153–166.

Amiri, M., Bahrami, F., & Janahmadi, M. (2012a). Functional contributions of astrocytes in synchronization of a neuronal network model. *Journal of Theoretical Biology*, *292*, 60–70.

Amiri, M., Bahrami, F., & Janahmadi, M. (2012b). Modified thalamocortical model: a step towards more understanding of the functional contribution ofastrocytes to epilepsy. *Journal of Computational Neuroscience*, *33*(2), 285–299.

Amiri, M., Bahrami, F., & Janahmadi, M. (2012c). On the role of astrocytes in epilepsy: a functional modeling approach. *Neuroscience Research*, *72*(2), 172–180.

Amiri, M., Hosseinmardi, N., Bahrami, F., & Janahmadi, M. (2013a). Astrocyte-neuron interaction as a mechanism responsible for generation of neural synchrony : a study based on odeling and experiments. *Journal of Computational Neuroscience*, *34*(3), 489–504.

Amiri, M., Montaseri, G., & Bahrami, F. (2013b). A phase plane analysis of neuron-astrocyte interactions. *Neural Networks*, *44*, 157–165.

Arthur, J. V., Merolla, P. A., Akopyan, F., Alvarez, R., Cassidy, A., Chandra, S., et al. (2012). Building block of a programmable neuromorphic substrate: a digital neurosynaptic core. In *The 2012 international joint conference on neural networks (IJCNN)* (pp. 1–8). IEEE.

Bonabi, S. Y., Asgharian, H., Safari, S., & Ahmadabadi, M. N. (2014). FPGA implementation of a biological neural network based on the Hodgkin–Huxley neuron model. *Frontiers in Neuroscience*, *8*.

Cassidy, A. S., Georgiou, J., & Andreou, A. G. (2013). Design of silicon brains in the nano-CMOS era: spiking neurons, learning synapses and neural architecture optimization. *Neural Networks*, *45*, 4–26.

Colangelo, A. M, Alberghina, L., & Papa, M. (2014). Astroglios is as a therapeutic target for neurodegenerative diseases. *Neuroscience Letters*, *565*, 59–64.

Corlew, R., Brasier, D. J., Feldman, D. E., & Philpot, B. D. (2008). Presynaptic NMDA receptors: newly appreciated roles in cortical synaptic function and plasticity. *The Neuroscientist*, *14*(6), 609–625.

Dallérac, G., Chever, O., & Rouach, N. (2013). How do astrocytes shape synaptic transmission? insights from electrophysiology. *Frontiers in Cellular Neuroscience*, *7*.

Di Castro, M. A., Chuquet, J., Liaudet, N., Bhaukaurally, K., Santello, M., Bouvier, D., et al. (2011). Local Ca^{2+} detection and modulation of synaptic release by astrocytes. *Nature Neuroscience*, *14*(10), 1276–1284.

Fellin, T. (2009). Communication between neurons and astrocytes: relevance to the modulation of synaptic and network activity. *Journal of Neurochemistry*, *108*(3), 533–544.

Fellin, T., Pascual, O., & Haydon, P. G. (2006). Astrocytes coordinate synaptic networks: balanced excitation and inhibition. *Physiology*, *21*(3), 208–215.

Frühbeis, C., Fröhlich, D., & Krämer-Albers, E. M. (2012). Emerging roles of exosomes in neuron–glia communication. *Membrane Physiology and Membrane Biophysics*, *3*, 119.

Frühbeis, C., Fröhlich, D., Kuo, W. P., Amphornrat, J., Thilemann, S., Saab, A. S., et al. (2013). Neurotransmitter-triggered transfer of exosomes mediates oligodendrocyte–neuron communication. *PLoS Biology*, *11*(7), e1001604.

Giugliano, M. (2009). Calcium waves in astrocyte networks:theory and experiments. *Frontiers in Neuroscience*, *3*(2), 160.

Halassa, M. M., Fellin, T., & Haydon, P. G. (2009). Tripartite synapses: roles for astrocytic purines in the control of synaptic physiology and behavior. *Neuropharmacology*, *57*(4), 343–346.

Indiveri, G., & Horiuchi, T. K. (2011). Frontiers in neuromorphic engineering. *Frontiers in Neuroscience*, *5*.

Izhikevich, E. M. (2003). Simple model of spiking neurons. *IEEE Transactions on Neural Networks*, *14*(6), 1569–1572.

Joshi, J., Parker, A.C., & Hsu, C.C. (2009). A carbon nanotube cortical neuron with spike-timing-dependent plasticity. In *Annual international conference of the IEEE engineering in medicine and biology society*, 2009. EMBC 2009 (pp. 1651–1654).

Joshi, J., Parker, A.C., & Tseng, K.C. (2011). An in-silico glial microdomain to invoke excitability in cortical neural networks. In *2011 IEEE international symposium on circuits and systems* (ISCAS) (pp. 681-684).

Koizumi, S. (2010). Synchronization of Ca^{2+} oscillations: involvement of ATP release in astrocytes. *FEBS Journal*, *277*(2), 286–292.

Kuga, N., Sasaki, T., Takahara, Y., Matsuki, N., & Ikegaya, Y. (2011). Large-scale calcium waves traveling through astrocytic networks in vivo. *The Journal of Neuroscience*, *31*(7), 2607–2614.

Li, W. X., Cheung, R. C., Chan, R. H., Song, D., & Berger, T. W. (2013). Real-time prediction of neuronal population spiking activity using FPGA. *IEEE Transactions on Biomedical Circuits and Systems*, *7*(4), 489–498.

Linne, M. L., & Jalonen, T. O. (2014). Astrocyte–neuron interactions: from experimental research-based models to translational medicine. *Progress in Molecular Biology and Translational Science*, *123*, 191.

López-Hidalgo, M., & Schummers, J. (2014). Corticalmaps: a role for astrocytes? *Current Opinion in Neurobiology*, *24*, 176–189.

Majumder, T., Pande, P.P., & Kalyanaraman, A. (2014). Hardware accelerators in computational biology: application, potential and challenges.

Min, R., Santello, M., & Nevian, T. (2012). The computational power of astrocyte mediated synaptic plasticity. *Frontiers in Computational Neuroscience*, *6*.

Misra, J., & Saha, I. (2010). Artificial neural networks in hardware: a survey of two decades of progress. *Neurocomputing*, *74*(1), 239–255.

Nazari, S., et al. (2014). A digital neurmorphic circuit for a simplified model of astrocyte dynamics. *Neuroscience Letters*, http://dx.doi.org/10.1016/j.neulet.2014.07.055.

Nedergaard, M., Ransom, B., & Goldman, S. A. (2003). New roles for astrocytes: redefining the functional architecture of the brain. *Trends in Neurosciences*, *26*(10), 523–530.

Newman, E. A. (2003). New roles for astrocytes: regulation of synaptic transmission. *Trends in Neurosciences*, *26*(10), 536–542.

Oberheim, N. A., Wang, X., Goldman, S., & Nedergaard, M. (2006). Astrocytic complexity distinguishes the human brain. *Trends in Neurosciences*, *29*(10), 547–553.

Papa, M., De Luca, C., Petta, F., Alberghina, L., & Cirillo, G. (2014). Astrocyte–neuron inter play in maladaptive plasticity. *Neuroscience and Biobehavioral Reviews*, *42*, 35–54.

Perea, G., Navarrete, M., & Araque, A. (2009). Tripartite synapses: astrocytes process and control synaptic information. *Trends in Neurosciences*, *32*(8), 421–431.

Pfeil, T., Grübl, A., Jeltsch, S., Müller, E., Müller, P., Petrovici, M. A., & Meier, K. (2013). Six networks on a universal neuromorphic computing substrate. *Frontiers in Neuroscience*, *7*.

Postnov, D. E., Koreshkov, R. N., Brazhe, N. A., Brazhe, A. R., & Sosnovtseva, O. V. (2009). Dynamical patterns of calcium signaling in a functional model of neuron–astrocyte networks. *Journal of Biological Physics*, *35*(4), 425–445.

Quilichini, P. P., & Bernard, C. (2012). Brain state-dependent neuronal computation. *Frontiers in Computational Neuroscience*, *6*.

Reato, D., Cammarota, M., Parra, L. C., & Carmignoto, G. (2012). Computational model of neuron-astrocyte interactions during focal seizure generation. *Frontiers in Computational Neuroscience*, *6*.

Rice, K. L., Bhuiyan, M. A., Taha, T. M., Vutsinas, C. N., & Smith, M. C (2009). FPGA implementation of Izhikevich spiking neural networks for character recognition. In *International conference on reconfigurable computing and FPGAs, 2009*, ReConFig'09. (pp. 451–456). IEEE.

Rusakov, D. A., Zheng, K., & Henneberger, C. (2011). Astrocytes as regulators of synaptic function: a quest for the Ca^{2+} master key. *The Neuroscientist*, 1073858410387304.

Sasaki, T., Kuga, N., Namiki, S., Matsuki, N., & Ikegaya, Y. (2011). Locally synchronized astrocytes. *Cerebral Cortex*, *21*(8), 1889–1900.

Sepulveda, C. A., Muñoz, J. A., Espinoza, J. R., Figueroa, M. E., & Melin, P. E. (2013). All-on-chip-frame based D-STATCOM control implementation in a low-cost FPGA. *IEEE Transactions on Industrial Electronics*, *60*(2), 659–669.

Silchenko, A. N., & Tass, P. A. (2008). Computational modeling of paroxysmal depolarization shifts in neurons induced by the glutamate release from astrocytes. *Biological Cybernetics*, *98*(1), 61–74.

Smith, K. (2010). Neuroscience: settling the great glia debate. *Nature*, *468*, 160–162.

Soleimani, H., Ahmadi, A., & Bavandpour, M. (2012). Biologically inspired spiking neurons: piecewise linear models and digital implementation. *IEEE Transactions on Circuits and Systems I: Regular Papers*, *59*(12), 2991–3004.

Terman, D., Rubin, J. E., Yew, A. C., & Wilson, C. J. (2002). Activity patterns in a model for the subthalamopallidal network of the basal ganglia. *The Journal of Neuroscience*, *22*(7), 2963–2976.

Volman, V., Ben-Jacob, E., & Levine, H. (2007). The astrocyte as a gatekeeper of synaptic information transfer. *Neural Computation*, *19*(2), 303–326.

Volterra, A., Liaudet, N., & Savtchouk, I. (2014). Astrocyte Ca^{2+} signalling: an unexpected complexity. *Nature Reviews Neuroscience*, *15*(5), 327–335.

Wang, R., Cohen, G., Stiefel, K. M., Hamilton, T. J., Tapson, J., & van Schaik, A. (2013). An FPGA implementation of a polychronous spiking neural network with delay adaptation. *Frontiers in Neuroscience*, *7*.

Wijekoon, J. H., & Dudek, P. (2012). VLSI circuits implementing computational models of neocortical circuits. *Journal of Neuroscience Methods*, *210*(1), 93–109.